Improved Rate-Energy Trade-off For SWIPT Using Chordal Distance Decomposition In Interference Alignment Networks

Improved Rate-Energy Trade-off For SWIPT Using Chordal Distance Decomposition In Interference Alignment Networks

Navneet Garg, Avinash Rudraksh, Govind Sharma, Tharmalingam Ratnarajah

Abstract

This paper investigates the simultaneous wireless information and power transfer (SWIPT) precoding scheme for K-user multiple-input-multiple-output (MIMO) interference channels (IC). In IC, interference alignment (IA) schemes provide optimal precoders to achieve full degrees-of-freedom (DoF) gain. To study a trade-off between harvested energy and sum rate, the transceiver design problem is suboptimally formulated in literature via convex relaxations, which is still computationally intensive, especially for battery limited nodes running on harvested energy. In this paper, we propose a systematic method using chordal distance (CD) decomposition to obtain the balanced precoding, which achieves the improved trade-off. Analysis shows that given the nonnegative value of CD, the achieved harvested energy for the proposed precoder is higher than that for perfect IA precoder. Moreover, energy constraints can be achieved, while maintaining a constant rate loss without losing DoFs via tuning the CD value and splitting factor. Simulation results verify the analysis and add that the IA schemes based on max-SINR or mean-squared error are better suited for SWIPT maximization than subspace or leakage minimization methods.

Index Terms

Chordal distance; interference alignment; power splitting; rate-energy trade-off; Simultaneous wireless information and power transfer (SWIPT).

I. Introduction

In wireless networks, energy consumption is one of the major issues due to increasing number of devices and the need for environment protection [1]. Green communications have attracted

N. Garg and T. Ratnarajah are with The University of Edinburgh, UK. A. Rudraksha and G. Sharma are with Indian Institute of Technology Kanpur, India. E-mails: {ngarg@ed.ac.uk, avinash.rudraksha@gmail.com, govind@iitk.ac.in, t.ratnarajah@ed.ac.uk}.

much interest from academia and industry. In the past few years, wireless energy harvesting (EH) has emerged as an important method to achieve green wireless communications [2]. In EH, the energy collected from the ambient environment can be utilized as a power supply for self-sustained wireless nodes [3], [4]. Since radio frequency (RF) signals carry energy, these signals can act as a new source for EH. Wireless power transfer (WPT) is becoming an important segment in future wireless communications. The experimental results in [5] show that a few microwatts of RF power can be harvested from broadcasting signals of TV stations, which are even located at several kms away. Thus, wireless EH system can be employed for energy constrained devices, implantable sensors, and smart wearables [6]. On the other hand, since RF signals also carry information in wireless networks, simultaneous information and power transfer (SWIPT) technology have attracted great research interests [7]–[11]. Some pioneering works on SWIPT have been done in [12], [13], where the rate-energy region has been characterized for single antenna point-to-point system. In [14], for multiple-input-multiple-output (MIMO) broadcast network, dedicated EH and information decoding (ID) receivers are used. The time switching duration (in time-division access) or power splitting (PS) ratio (in frequency-division access) is computed using iterative convexified algorithm in [15]. [16] proposes the quantized CSI feedback to improve EH, and derives the trade-off between EH duration and ID.

Further, for interference channels (ICs), interference is one of the most fundamental and challenging aspects. Regarding interference cancellation, from the last decade, interference alignment (IA) has emerged as a promising solution for MIMO wireless networks. Under certain conditions, IA has been shown to be degree of freedom (DoF) optimal for ICs [17]. In IA, the precoders at the sources and the decoders at the destinations are employed to align and cancel the interfering signal from other users [17]. To design these IA precoders and decoders, several iterative algorithms have been investigated in the literature, such as signal-to-interference-plus-noise-ratio (SINR) maximization, leakage minimization [18], [19], mean squared error (MSE) minimization [20], [21], alternating minimization [22], etc. These IA algorithms assume channel state information (CSI) available at the sources to compute the IA precoders. In frequency division duplexed (FDD) systems, this information is obtained at the sources using CSI feedback either in quantized or in analog form [23]–[27]. In quantized CSI feedback, the linear rate scaling is maintained at a given signal-to-noise-ratio (SNR), only if the number of bits are scaled proportional to SNR [26], [28]–[30]. For analog feedback, a constant rate-loss has been observed at medium-to-high SNR regime, i.e., without any loss of DoFs.

Next, for IA networks, the interference component is canceled at each receiver to separate out the desired signal. However, before interference nulling, the received signal can be split, and the interference power can be utilized for harvesting energy. A review of SWIPT schemes is given as follows. In [31] with 2-users IC, different possible transmission strategies are defined for time-switching (TS) receivers. [32] collaboratively obtains the optimal TS duration for 2-user IC, which is further extended to K-users via introducing user-groups. In [33] for multiple-input-single-output (MISO) IC, PS ratio and power allocation is obtained to show that maximal ratio transmission (MRT) based precoding outperforms zero-forcing (ZF) in terms of EH. [34] improves harvested energy and its consumption problem via power allocation, while keeping fairness among users. In [35], [36], antenna selection is used for EH improvements. In [37], an upper bound on EH is derived. In [11], [38], semi-definite relaxation technique is leveraged to obtain suboptimal solutions via convexifying the joint transceiver design problem. In [1], power splitting algorithm is proposed to maximize a linear-sum of rate and energy objectives, where the coefficient of the linear-sum decides the weight of these objectives.

A. Contributions

In this paper, a systematic precoding approach for SWIPT maximization is investigated for the K-user MIMO-IC. From the above review, it can be noted that in IA-SWIPT literature, authors have posed the optimization problem as a linear sum of sum rate and harvested energy, and sub-optimum solution have been computed convex relaxation tools [11], [38]. In this work, using chordal distance (CD) decomposition, a systematic method is presented to obtain the balanced precoding, which improves the trade-off between sum rate and harvested energy. The proposed precoder, which is the key for the rate-energy trade-off, can be obtained for the maximum harvested energy, or to get the maximum sum rate via tuning the value of chordal distance. EH analysis shows the guaranteed improvement of energy for the proposed formulation. Simulation results for different IA methods have been compared. These results show that the IA methods utilizing direct channels, such as MMSE and max-SINR algorithms, provide the better harvested power than that of the IA methods, which does not utilize direct channels in the precoder design including subspace method or leakage minimization algorithm. Analog feedback automatically chooses the chordal distance, which provides better EH and linear sum rate scaling at high SNR. On the other hand, with quantized feedback, increasing the size of codebook increases harvested

energy, while suffering DoF losses. In summary, the contribution of this paper can be listed as follows:

1) Rate energy balanced precoding: First, the maximum harvested energy achievable is obtained using the precoders $\mathbf{V}^{EH}$, which defines the upper limit achievable on EH. Then, we systematically derive the balanced precoding scheme to improve SWIPT trade-off using CD decomposition. Beyond the upper limit i.e., when the CD value between IA and the proposed precoder is chosen greater than the CD value between the IA precoder and $\mathbf{V}^{EH}$, the precoder $\mathbf{V}^{EH}$ provides the better sum rates. It is also worth noting that the proposed method is much computationally efficient, as compared to semi-definite programming.

2) Simple parameter design for constant rate loss: We analyze the upper and lower bounds on the harvested energy. Tuning CD and PS ratio, the trade-off between sum rate and harvested energy for IA networks can be observed. Further, the cases of analog and quantized feedback are analyzed, where the CD value is automatically set based on the feedback transmission power in the analog feedback, and based on the size of codebook in the quantized feedback. In both cases, harvested energy is shown to improve than that in the case of IA precoder. Moreover, it is shown that it is possible to obtain constant rate loss (i.e., linear sum rate scaling with respect to SNR), while achieving the desired harvested energy threshold.

3) Which is the best IA scheme for harvesting? : Simulation results verify the improvements and limits of balanced precoder via the plots for rate-energy regions, and show that MSE based IA schemes are better suited for SWIPT trade-offs than subspace or leakage minimization schemes. Both analog and quantized feedback improves the harvested energy, while achieving a constant rate loss in the former case, and getting the rate loss proportional to codebook size in the latter case.

Organization: The interference channel model is given in section II. The next sections III and IV present energy optimized precoding and the proposed balanced precoding, followed by the the cases of analog and quantized feedback in section V. Simulation results are presented in Section VI. Section VII concludes the work.

Notations: Scalars, vectors and matrices are represented by the lower case (a), lower case bold face ($\mathbf{a}$) and upper case bold face ($\mathbf{A}$) letters respectively. Conjugate, transpose, Hermitian transpose and Kronecker product of matrices are denoted by $(\cdot)^*$, $(\cdot)^T$, $(\cdot)^\dagger$ and $\otimes$ respectively. $\mathcal{CN}(\mu, \mathbf{R})$ represents a circularly symmetric complex Gaussian random vector with mean μ and covariance matrix $\mathbf{R}$. The notations $\|\cdot\|$ and $\|\cdot\|_F$ denote the l_2 norm and Frobenious

norm. vec($\mathbf{X}$) denotes the column-wise vector representation of matrix $\mathbf{X}$. $\mathcal{D}(\mathbf{A}_i)$ denotes a block diagonal matrix with matrices $\mathbf{A}_i$ as its block diagonal components. $\mathbb{O}(\mathbf{X})$ denotes the orthonormal part of the QR decomposition of $\mathbf{X}$ [20]. $\mathbf{X}$ is unitary means $\mathbf{X}\mathbf{X}^\dagger = \mathbf{X}^\dagger\mathbf{X} = \mathbf{I}$. $\lambda_{\max}(\mathbf{A})$, $\nu_{\max}(\mathbf{A})$, $\nu_{1:d}(\mathbf{A})$ denote the maximum eigenvalue, the corresponding eigenvector of $\mathbf{A}$, and the matrix with columns being the eigenvectors corresponding to d-largest eigenvalues. δ_{ij} is Kronecker delta, which takes value 1 when $i = j$ and 0 otherwise.

II. System Model

Consider an IA-feasible MIMO interference channel [39]–[41] with K users. Each user pair has M transmit antennas, N receive antennas and d independent data streams to be communicated. This system is represented by the notation $(M \times N, d)^K$ [39]. Let $\mathbf{x}_k$ of size $d \times 1$ denote the transmit vector of the k^{th} user, distributed as $\mathcal{CN}(\mathbf{0}, p_k\mathbf{I}_d)$ with power $p_k = \frac{P_k}{d}$, where $P_k = \text{tr}\left(\mathbb{E}\left\{\mathbf{x}_k\mathbf{x}_k^\dagger\right\}\right), \forall k$. The MIMO channel matrix between the j^{th} transmitter and k^{th} receiver is denoted by $\mathbf{H}_{kj} \in \mathbb{C}^{N\times M}$. The received signal at the k^{th} user is given as

$$\mathbf{y}_k = \mathbf{H}_{kk}\mathbf{V}_k\mathbf{x}_k + \sum_{j\neq k}\mathbf{H}_{kj}\mathbf{V}_j\mathbf{x}_j + \mathbf{n}_k, \tag{1}$$

where the precoder $\mathbf{V}_k = [\mathbf{v}_{k1}, \mathbf{v}_{k2}, \ldots, \mathbf{v}_{kd}] \in \mathbb{C}^{M\times d}$ is an orthonormal matrix employed at the transmitter and satisfies the constraint $\mathbf{v}_{ki}^\dagger\mathbf{v}_{kj} = \delta_{ij}$, $\forall k$, i, j. The quantity $\mathbf{n}_k$ denotes zero mean additive white Gaussian noise (AWGN), distributed as $\mathcal{CN}(\mathbf{0}, \sigma^2\mathbf{I}_N)$. The first term in the above equation represents the desired signal component, while the second and third terms correspond to the interference and noise components respectively.

A. Information Decoding

Each receiver adaptively splits the received signal into two flows, i.e., one part goes to the RF-EH circuits for energy storage, while the other part is converted to a baseband signal for information decoding. The received signal $\mathbf{y}_k$ is fed into a power splitting device with a power splitting ratio $\rho_k \in [0, 1]$, which denotes the portion of the received signal power assigned for ID, and the remaining $(1-\rho_k)$ portion allocated for harvesting energy. Before ID, the split signal is further corrupted by additional circuit noise $\mathbf{w}_k$, due to the non-ideal splitters, non-ideal RF-

to-baseband signal conversion, and thermal noise [11]. Therefore, after splitting, the signal for ID can be expressed as

$$\mathbf{y}_k^{ID} = \sqrt{\rho_k}\mathbf{y}_k + \mathbf{w}_k, \tag{2}$$

$$= \sqrt{\rho_k}\left(\mathbf{H}_{kk}\mathbf{V}_k\mathbf{x}_k + \sum_{j\neq k}\mathbf{H}_{kj}\mathbf{V}_j\mathbf{x}_j + \mathbf{n}_k\right) + \mathbf{w}_k, \tag{3}$$

where $\mathbf{w}_k \sim \mathcal{CN}(\mathbf{0}, \delta^2\mathbf{I}_N)$ represents the power splitting circuit noise vector at receiver k. It can be noted that the above equation results in the effective noise of $\mathbf{n}_k + \frac{\mathbf{w}_k}{\sqrt{\rho_k}} \sim \mathcal{CN}\left(\mathbf{0}, \sigma_{ID}^2\mathbf{I}_N\right)$, where $\sigma_{ID}^2 = \sigma^2\left(1 + \frac{\delta^2}{\rho_k\sigma^2}\right)$. Further, the signal is processed via a linear receiver $\mathbf{U}_k$, where $\mathbf{U}_k = [\mathbf{u}_{k1}, \mathbf{u}_{k2}, \ldots, \mathbf{u}_{kd}] \in \mathbb{C}^{N\times d}$ denotes an orthonormal decoding matrix, and can be obtained from minimizing MSE [20], [27].

1) IA feasibility: In the above equation, to cancel the interference component and preserve the desired signal, the precoders $\{\mathbf{V}_k, \forall k\}$ and the decoders $\{\mathbf{U}_k, \forall k\}$ should be chosen to satisfy the following equations

$$\mathbf{U}_k^\dagger\mathbf{H}_{kj}\mathbf{V}_j = \mathbf{0}, \forall j \neq k \forall k, \tag{4}$$

$$\text{rank}(\mathbf{U}_k^\dagger\mathbf{H}_{kk}\mathbf{V}_k) = d_k, \forall k. \tag{5}$$

In order to find possible solutions for $\{\mathbf{V}_k, \forall k\}$ and $\{\mathbf{U}_k, \forall k\}$, the system must be IA-feasible. Characterizations of IA-feasible systems are given in [39]–[41]. [39], and others [42]–[44] have demonstrated that feasible systems must necessarily be proper, which requires the number of equations in (4) to be lower than the number of variables, i.e., $M+N-(K+1)d \geq 0$. In addition to the proper condition, [40] has shown that feasibility can be verified by testing the surjectivity of the mapping proposed therein. More specifically, [41] and [42] have shown that a proper system is feasible when either M or N is divisible by d, or the system is symmetric, i.e., $M = N$. Further, [45] presents a uniqueness condition and ensures the IA-feasibility and the global maximum sum rate (or minimum MSE). Thus, we utilize the condition $M + N - (K + 2)d \geq 0$ along with the IA algorithm from [45] to get the IA-solution.

2) Sum rate: At the k^{th} destination, the resulting sum rate can be expressed as

$$R_k = \log_2\left|\mathbf{I}_d + p_k\bar{\mathbf{H}}_{kk}\bar{\mathbf{H}}_{kk}^\dagger\left(\sigma_{ID}^2\mathbf{I}_d + \sum_{\forall j\neq k} p_j\bar{\mathbf{H}}_{kj}\bar{\mathbf{H}}_{kj}^\dagger\right)^{-1}\right|, \tag{6}$$

where $\bar{\mathbf{H}}_{kj} = \mathbf{U}_k^{\dagger}\mathbf{H}_{kj}\mathbf{V}_j$. If the interference components are perfectly canceled i.e. $\bar{\mathbf{H}}_{kj} = \mathbf{0}, \forall j \neq k$, we have

$$R_{k,per} = \log_2 \left| \mathbf{I}_d + \frac{P_k}{d\sigma_{ID}^2} \bar{\mathbf{H}}_{kk} \bar{\mathbf{H}}_{kk}^{\dagger} \right| \tag{7}$$

$$= \sum_{i=1}^{d} \log_2 \left(1 + \frac{P_k}{d\sigma_{ID}^2} |\sigma_{kki}|^2 \right), \tag{8}$$

where $\sigma_{kki} \forall i = 1, \ldots, d$ are the singular values of $\bar{\mathbf{H}}_{kk}$.

B. Harvested Energy

The second part of the splitted received signal for energy storage at receiver k can be written as

$$\mathbf{y}_k^{EH} = \sqrt{\bar{\rho}_k}\mathbf{y}_k, \forall k, \tag{9}$$

with $\bar{\rho}_k = 1 - \rho_k$. The corresponding average harvested energy that can be stored at receiver k can be expressed as

$$Q_k = \zeta \mathbb{E}\left\{ \|\mathbf{y}_k^{EH}\|^2 \right\} \tag{10}$$

$$\approx \zeta \bar{\rho}_k \sum_{j=1}^{K} \frac{P_j}{d} \|\mathbf{H}_{kj}\mathbf{V}_j\|_F^2, \tag{11}$$

where $0 < \zeta < 1$ represents the power conversion efficiency for EH, which is assumed to be equal for all receivers in the paper. Note that the noise power $\zeta(1-\rho_k)N\sigma^2$ is negligible and hence, is omitted in the above equation.

III. Energy Optimized Precoding Method

In this section, we first derive the precoders achieving the maximum harvested energy. Subsequently, the rate-loss is analyzed via chordal distance.

A. Precoding for the maximum EH

The problem of maximizing the total harvested energy with respect to precoders, subject to orthogonality constraint on the precoders can be written as

$$\left\{ \mathbf{V}_j^{EH}, \forall j \right\} = \arg\max_{\mathbf{V}_j, \forall j} \sum_k \zeta \bar{\rho}_k \sum_j \frac{P_j}{d} \|\mathbf{H}_{kj}\mathbf{V}_j\|_F^2 \tag{12a}$$

$$\text{subject to } \|\mathbf{V}_j\|_F^2 \leq d, \forall j. \tag{12b}$$

The above problem can be decoupled and the solution of the j^{th} precoder $\mathbf{V}_j$ can be obtained by the dominant eigenvectors of the $\sum_k \bar{\rho}_k \mathbf{H}_{kj}^{\dagger}\mathbf{H}_{kj}$ corresponding to d maximum eigenvalues i.e.,

$$\begin{aligned}\mathbf{V}_j^{EH} &= \arg \max_{\|\mathbf{V}_j\|_F^2 \leq d} \text{tr}\left(\mathbf{V}_j^{\dagger}\mathbf{H}_j^{\dagger}\mathbf{H}_j\mathbf{V}_j\right) \\ &= \nu_{1:d}\left[\mathbf{H}_j^{\dagger}\mathbf{H}_j\right] = \mathbf{W}_j^{[1]},\end{aligned} \tag{13}$$

where $\mathbf{H}_j^T = \left[\bar{\rho}_1\mathbf{H}_{1j}^T, \ldots, \bar{\rho}_K\mathbf{H}_{Kj}^T\right]$ denotes a stack of the channel matrices, and $\mathbf{W}_j^{[1]}$ is computed via the eigenvalue decomposition (EVD) i.e.,

$$\mathbf{H}_j^{\dagger}\mathbf{H}_j = \sum_k \bar{\rho}_k \mathbf{H}_{kj}^{\dagger}\mathbf{H}_{kj} = \mathbf{W}_j\mathbf{\Lambda}_j\mathbf{W}_j^{\dagger}, \tag{14}$$

with $\mathbf{W}_j = \left[\mathbf{W}_j^{[1]}, \mathbf{W}_j^{[2]}\right]$ and $\mathbf{\Lambda}_j = \mathcal{D}\left(\lambda_{ji}, i = 1\ldots, M\right)$ such that $\lambda_{j1} \geq \ldots \geq \lambda_{jM}$ being in the descending order. Note that $\mathbf{W}_j^{[1]}$ and $\mathbf{W}_j^{[2]}$ are orthonormal matrices of size $M \times d$ and $M \times M - d$, respectively. To analyze the effect of the precoding scheme, we utilize chordal distance and its decomposition, which are defined in the following.

B. Chordal Distance

Definition 1. Let $\mathbf{V}, \hat{\mathbf{V}} \in \mathbb{C}^{M\times d}$ be two orthonormal matrices such that $\hat{\mathbf{V}}^{\dagger}\hat{\mathbf{V}} = \mathbf{V}^{\dagger}\mathbf{V} = \mathbf{I}_d$. The chordal distance between these matrices can be defined as

$$d_c^2(\mathbf{V}, \hat{\mathbf{V}}) \;=\; \frac{1}{2}\|\mathbf{V}\mathbf{V}^{\dagger} - \hat{\mathbf{V}}\hat{\mathbf{V}}^{\dagger}\|_F^2 = d - \|\mathbf{V}^{\dagger}\hat{\mathbf{V}}\|_F^2. \tag{15}$$

Note that the matrices $\mathbf{V}$ and $\hat{\mathbf{V}}$ represent d dimensional subspaces of M dimensional space, i.e., $\mathbf{V}$ and $\hat{\mathbf{V}}$ lie on a Grassmannian manifold $\mathcal{G}_{M,d}$, which is a collection of all such d dimensional subspaces. The chordal distance represents the distance between the subspaces spanned by these matrices. Thus, two orthonormal matrices who represent the same column space, will have zero CD between them. CD between two unit-norm vectors (say $\mathbf{v}_1, \mathbf{v}_2 \in \mathcal{G}_{M,1}$), is equivalent to computing the inner-product between them, i.e. $1 - \left|\mathbf{v}_1^{\dagger}\mathbf{v}_2\right|^2$. Further, given two matrices in $\mathcal{G}_{M,d}$, one matrix can be expressed into the other one using the CD decomposition lemma from [24, Lemma 1]. The following lemma states the modified CD decomposition, where the modification comes from splitting the null space of dimension $M - d$ into a product of two variables.

Lemma 2. *The two matrices* $\hat{\mathbf{V}}$ *and* $\mathbf{V}$ *(such that* $\hat{\mathbf{V}}^\dagger\hat{\mathbf{V}} = \mathbf{V}^\dagger\mathbf{V} = \mathbf{I}_d$*) admits the following decomposition [24, Lem 1]*

$$\mathbf{V} = \hat{\mathbf{V}}\mathbf{X}\mathbf{Y} + \hat{\mathbf{V}}^{null}\mathbf{S}\mathbf{Z}, \tag{16}$$

where $\mathbf{V}$, $\hat{\mathbf{V}} \in \mathbb{C}^{M\times d}$, $\hat{\mathbf{V}}_j^{null} = null(\hat{\mathbf{V}}_j) \in \mathbb{C}^{M-d\times d}$, $\mathbf{X} \in \mathbb{C}^{d\times d}$ *and* $\mathbf{S} \in \mathbb{C}^{M-d\times d}$ *are orthonormal matrices,* $\mathbf{Y}$, $\mathbf{Z} \in \mathbb{C}^{d\times d}$ *are upper triangular matrices with positive diagonal elements satisfying*

$$\mathrm{tr}(\mathbf{Z}^\dagger\mathbf{Z}) = d_c^2(\mathbf{V}, \hat{\mathbf{V}}) \tag{17}$$

$$\mathbf{Y}^\dagger\mathbf{Y} = \mathbf{I}_d - \mathbf{Z}^\dagger\mathbf{Z}, \tag{18}$$

Moreover, $\mathbf{X}$ *and* $\mathbf{Y}$ *are distributed independent of each other, as is the pair* $\mathbf{S}$ *and* $\mathbf{Z}$*.*

Proof: A short proof is included in Appendix-A [24]. ■

Note that this decomposition requires $M \geq 2d$, which is the case in interference alignment, wherein at least $2d$ dimensions are required i.e., at least d dimensions for the desired signal and the remaining for the interference.

Corollary 3. *For IC, if two sets of precoders have zero chordal distances, then the resulting rate and the harvested energy are same.*

Proof: Let $\mathbf{V}_j$ and $\hat{\mathbf{V}}_j$ be two set of precoders such that $d_c^2\left(\mathbf{V}_j, \hat{\mathbf{V}}_j\right) = 0, \forall j$, i.e., from Lemma 2, $\mathbf{V}_j = \hat{\mathbf{V}}_j\mathbf{X}_j\mathbf{Y}_j$ with $\mathbf{X}_j\mathbf{X}_j^\dagger = \mathbf{Y}_j\mathbf{Y}_j^\dagger = \mathbf{I}_d, \forall j$. The sum rate and the harvested energy will be same due to the fact that the matrices with the zero chordal distances are related by a unitary matrix, which cannot change the value of the product $\mathbf{V}_j\mathbf{V}_j^\dagger = \hat{\mathbf{V}}_j\hat{\mathbf{V}}_j^\dagger, \forall j$, the product $\bar{\mathbf{H}}_{kj}\bar{\mathbf{H}}_{kj}^\dagger, \forall j, k$ and the norm $\|\mathbf{H}_{kj}\mathbf{V}_j\|_F^2, \forall j, k$. ■

Note that the two different orthogonal matrices with zero chordal distance will be termed as *equivalent* matrices; however, they cannot be considered as the same matrix.

Corollary 4. *Given the chordal distance* z *and an orthogonal matrix* $\mathbf{V}$*. Then, in obtaining the displacement precoder (with respect to* $\mathbf{V}$*) via the CD decomposition, the matrices* $\mathbf{Y}$ *and* $\mathbf{Z}$ *can be relaxed to diagonal matrices as*

$$\mathbf{V}_D = \mathbf{V}\mathbf{X}\Sigma_Y + \mathbf{V}^{null}\mathbf{S}\Sigma_Z, \tag{19}$$

where Σ_Y *and* Σ_Z *are diagonal matrices such that* $\Sigma_Y^2 = \mathbf{I}_d - \Sigma_Z^2$*.*

Proof: From the CD decomposition, the desired displacement matrix can be computed as $\mathbf{V}\bar{\mathbf{X}}\mathbf{Y} + \mathbf{V}^{\text{null}}\bar{\mathbf{S}}\mathbf{Z}$, where $\bar{\mathbf{X}}, \mathbf{Y}, \bar{\mathbf{S}}, \mathbf{Z}$ will be computed to satisfy the constraint in Lemma 2. The chordal distance between this matrix and $\mathbf{V}$ can be written as

$$z = d_c^2\left(\mathbf{V}\bar{\mathbf{X}}\mathbf{Y} + \mathbf{V}^{\text{null}}\bar{\mathbf{S}}\mathbf{Z}, \mathbf{V}\right) \tag{20a}$$

$$\overset{(a)}{=} d_c^2\left(\mathbf{V}\bar{\mathbf{X}}\mathbf{U}_Y\Sigma_Y\mathbf{V}_Y^\dagger + \mathbf{V}^{\text{null}}\bar{\mathbf{S}}\mathbf{U}_Z\Sigma_Z\mathbf{V}_Y^\dagger, \mathbf{V}\right) \tag{20b}$$

$$\overset{(b)}{=} d_c^2\left(\mathbf{V}\mathbf{X}\Sigma_Y + \mathbf{V}^{\text{null}}\mathbf{S}\Sigma_Z, \mathbf{V}\mathbf{V}_Y\right) \tag{20c}$$

$$\overset{(c)}{=} d_c^2\left(\mathbf{V}\mathbf{X}\Sigma_Y + \mathbf{V}^{\text{null}}\mathbf{S}\Sigma_Z, \mathbf{V}\right) \tag{20d}$$

$$= d_c^2\left(\mathbf{V}_D, \mathbf{V}\right), \tag{20e}$$

where in (a), the SVD of $\mathbf{Z} = \mathbf{U}_Z\Sigma_Z\mathbf{V}_Y^\dagger$ and $\mathbf{Y} = \mathbf{U}_Y\Sigma_Y\mathbf{V}_Y^\dagger$ with the same right singular vectors due to the constraint $\mathbf{Y}^\dagger\mathbf{Y} = \mathbf{I}_d - \mathbf{Z}^\dagger\mathbf{Z}$, and $\mathbf{S} = \bar{\mathbf{S}}\mathbf{U}_Z$, $\mathbf{X} = \bar{\mathbf{X}}\mathbf{U}_Y$ are substituted; in (b), the unitary matrix $\mathbf{V}_Y$ is multiplied into both arguments, since the resulting chordal distance is unchanged for unitary multiplication, as in (c). The above shows that $\mathbf{Z}$ and $\mathbf{Y}$ can be relaxed to a diagonal matrices. ■

C. Rate loss upper bound for EH based precoding

With the maximum EH based precoding in (13), the resultant maximum harvested energy can be written as the sum of the first d dominant eigenvalues of $\sum_k \bar{\rho}_k\mathbf{H}_{kj}^\dagger\mathbf{H}_{kj}$. Note that the precoding in (13) is an independent precoding scheme, which does not consider the effect of interference on information decoding. However, the obtained precoders may partially align the interference. This partial alignment can be measured using the chordal distance between the ideal IA precoders and EH precoders as

$$z_j^{EH} = d_c^2(\mathbf{V}_j, \mathbf{V}_j^{EH}), \forall j,$$

where $\mathbf{V}_j, \forall j$ stands for IA-precoders. It can be noted that the above chordal distance represents the displacement of $\mathbf{V}_j^{EH}$ with respect to $\mathbf{V}_j$, and it does not depend on SNR values. The more the distance, the more will be interference. Therefore, in the rate-energy trade-off, it is essential to specify the allowable interference in the system, which can be characterized in the following result from our analysis in [27].

Lemma 5. *(Rate Loss Upper Bound (RLUB)) In an interference channel $(M \times N, d)^K$, the usage of imperfect precoder instead of IA precoder at the sources incurs the rate loss ΔR_k, whose expected value can be upper bounded for the k^{th} receiver as*

$$\mathbb{E}\left\{\Delta R_k\right\} < d \log_2 \left(1 + \frac{P}{\sigma^2} \frac{(K-1)M}{d(M-d)} z\right), \tag{21}$$

with $z = \mathbb{E} d_c^2(\mathbf{V}_k, \hat{\mathbf{V}}_k)$ being the average chordal distance between the IA precoder and the imperfect one.

Proof: Proof is given in our previous work [27, Lemma 4]. Note that the expectation is with respect to the channel matrices $\mathbf{H}_{kj}, \forall j$. ■

D. Problem Formulation

For the SWIPT precoding in literature [6], [46], authors have formulated an optimization problem in which a linear sum of the sum rate and sum harvested energy is maximized subjected to the desired harvested energy $\bar{Q}$, and precoder constraints as

$$\max_{\mathbf{V}_j, \forall j} \sum_k R_k\left(\mathbf{V}_j, \forall j \middle| \mathbf{H}_j\right) + \nu Q_k\left(\mathbf{V}_j, \forall j \middle| \mathbf{H}_j\right) \tag{22a}$$

$$\text{subject to } Q_k \geq \bar{Q}, \forall k, \|\mathbf{V}_j\|_F^2 \leq d, \forall j, \tag{22b}$$

where ν is the weight controlling the preferred objective. Note that the above two are opposing objectives, i.e. if the sum rate is maximized, the harvested energy is reduced, and if the sum harvested energy is maximized, the sum rate degrades. To provide a balanced precoder, we start with the sum rate optimal precoder i.e. IA precoder $\mathbf{V}_j$, and degrade this precoder in such a way that the degraded precoder satisfies the required harvested energy constraint.

In general, if we degrade the IA precoder, it will result in severe rate loss, causing the loss in degrees of freedom. Thus, to degrade the IA precoder in a systematic manner, we employ the chordal distance decomposition, in which the value of chordal distance decides the degradation in the precoder. Therefore, given the chordal distance and IA precoder, the balanced precoder is obtained in the following section.

IV. Proposed Balanced precoding Method

A. Optimization Problem

Given the IA precoders $\{\mathbf{V}_j, \forall j\}$ and the value of chordal distance $\{z_j, \forall j\}$, we can now focus on maximizing the harvested energy, since the sum rate obtained with a given chordal distance

is fixed and will be systematically degraded from the sum rate with the perfect IA precoder. Thus, the j^{th} balanced precoder can be expressed using CD decomposition in Corollary 4 as

$$\mathbf{V}_j^{BAL} = \mathbf{V}_j\mathbf{X}_j\mathbf{Y}_j + \mathbf{V}_j^{\text{null}}\mathbf{S}_j\mathbf{Z}_j, \tag{23}$$

where $\mathbf{Y}_j$ and $\mathbf{Z}_j$ are diagonal matrices from corollary 4; the matrices $\mathbf{X}_j$ and $\mathbf{Z}_j$ are obtained in the following to maximize the energy; and $\mathbf{V}_j^{\text{null}}$ represents the left null space of $\mathbf{V}_j$, i.e., $\mathbf{V}_j^{\text{null}} = \text{null}(\mathbf{V}_j) \in \mathcal{G}_{M,M-d}$ and $\mathbf{V}_j^{\text{null}\dagger}\mathbf{V}_j = \mathbf{0}$.

The optimization problem to find the balanced precoding to maximize the total harvested energy can be cast as

$$\max_{\mathbf{S}_j,\mathbf{Z}_j,\mathbf{X}_j,\mathbf{Y}_j,\forall j} \sum_k \zeta\bar{\rho}_k \sum_j \frac{P_j}{d}\|\mathbf{H}_{kj}\mathbf{V}_j^{BAL}\|_F^2 \tag{24a}$$

$$\text{subject to } \mathbf{V}_j^{BAL} = \mathbf{V}_j\mathbf{X}_j\mathbf{Y}_j + \mathbf{V}_j^{\text{null}}\mathbf{S}_j\mathbf{Z}_j, \forall j, \tag{24b}$$

$$\text{tr}\left(\mathbf{Z}_j\mathbf{Z}^\dagger\right) = \text{tr}\left(\mathbf{I} - \mathbf{Y}_j\mathbf{Y}_j^\dagger\right) \leq z_j, \forall j \tag{24c}$$

$$\mathbf{Z}_j, \mathbf{Y}_j \text{ are diagonal matrices}, \forall j, \tag{24d}$$

$$\mathbf{X}_j^\dagger\mathbf{X}_j = \mathbf{X}_j\mathbf{X}_j^\dagger = \mathbf{I}, \forall j, \tag{24e}$$

$$\mathbf{S}_j^\dagger\mathbf{S}_j = \mathbf{I}, \forall j. \tag{24f}$$

Note that the above problem can be decoupled for each j^{th} precoder as

$$\max_{\mathbf{S}_j,\mathbf{Z}_j,\mathbf{X}_j,\mathbf{Y}_j} \left\|\mathbf{H}_j\mathbf{V}_j^{BAL}\right\|_F^2 \tag{25a}$$

$$\text{subject to } \mathbf{V}_j^{BAL} = \mathbf{V}_j\mathbf{X}_j\mathbf{Y}_j + \mathbf{V}_j^{\text{null}}\mathbf{S}_j\mathbf{Z}_j, \tag{25b}$$

$$\text{tr}\left(\mathbf{Z}_j\mathbf{Z}^\dagger\right) = \text{tr}\left(\mathbf{I} - \mathbf{Y}_j\mathbf{Y}_j^\dagger\right) \leq z_j, \tag{25c}$$

$$\mathbf{Z}_j, \mathbf{Y}_j \text{ are diagonal matrices}, \tag{25d}$$

$$\mathbf{X}_j^\dagger\mathbf{X}_j = \mathbf{X}_j\mathbf{X}_j^\dagger = \mathbf{I}, \tag{25e}$$

$$\mathbf{S}_j^\dagger\mathbf{S}_j = \mathbf{I}. \tag{25f}$$

The solution of the above problem is obtained as follows. First, $\mathbf{S}_j$ is computed, followed by the computation of $\mathbf{Z}_j$ and $\mathbf{X}_j$, which are derived using both iterative and non-iterative approaches.

B. Getting $\mathbf{S}_j$

Using the triangle inequality, the objective function in (25a) can be upper bounded as

$$\begin{aligned}&\left\|\mathbf{H}_j\left(\mathbf{V}_j\mathbf{X}_j\mathbf{Y}_j+\mathbf{V}_j^{\text{null}}\mathbf{S}_j\mathbf{Z}_j\right)\right\|_F\\&\leq\left\|\mathbf{H}_j\mathbf{V}_j\mathbf{X}_j\mathbf{Y}_j\right\|_F+\left\|\mathbf{H}_j\mathbf{V}_j^{\text{null}}\mathbf{S}_j\mathbf{Z}_j\right\|_F,\end{aligned}\tag{26}$$

where the equality occurs when both $\mathbf{H}_j\mathbf{V}_j\mathbf{X}_j\mathbf{Y}_j$ and $\mathbf{H}_j\mathbf{V}_j^{\text{null}}\mathbf{S}_j\mathbf{Z}_j$ are in the same direction or proportional to each other. Since both the precoder $\mathbf{V}_j$ and its null space $\mathbf{V}_j^{\text{null}}$ are present in the above norm expression, the equality cannot be achieved for $z_j>0$ or $\mathbf{Z}_j\neq\mathbf{0}$. Best efforts can be done to align these matrices using the following optimization problem as

$$\min_{\mathbf{S}_j,\mathbf{Z}_j,\mathbf{X}_j,\mathbf{Y}_j} d_c^2\left(\mathbb{O}\left(\mathbf{H}_j\mathbf{V}_j\mathbf{X}_j\mathbf{Y}_j\right),\mathbb{O}\left(\mathbf{H}_j\mathbf{V}_j^{\text{null}}\mathbf{S}_j\mathbf{Z}_j\right)\right),\tag{27a}$$

$$\overset{(a)}{=}\min_{\mathbf{S}_j} d_c^2\left(\mathbb{O}\left(\mathbf{H}_j\mathbf{V}_j\right),\mathbb{O}\left(\mathbf{H}_j\mathbf{V}_j^{\text{null}}\mathbf{S}_j\right)\right),\tag{27b}$$

$$\overset{(b)}{=}\max_{\mathbf{S}_j^\dagger\mathbf{S}_j=\mathbf{I}}\text{tr}\left[\mathbf{D}_{Vj}\mathbf{V}_j^\dagger\mathbf{H}_j^\dagger\mathbf{H}_j\mathbf{V}_j^{\text{null}}\mathbf{S}_j\mathbf{D}_{Vnj}\right],\tag{27c}$$

where in (a), the orthogonalization property is used, since both matrices represent the same basis of the column space; in (b), the definition of chordal distance, $\mathbb{O}\left(\mathbf{A}\right)=\mathbf{A}\left(\mathbf{A}^\dagger\mathbf{A}\right)^{-1/2}$, $\mathbf{D}_{Vj}=\left(\mathbf{V}_j^\dagger\mathbf{H}_j^\dagger\mathbf{H}_j\mathbf{V}_j\right)^{-1/2}$, and $\mathbf{D}_{Vnj}=\left(\mathbf{S}_j^\dagger\mathbf{V}_j^{\text{null}\dagger}\mathbf{H}_j^\dagger\mathbf{H}_j\mathbf{V}_j^{\text{null}}\mathbf{S}_j\right)^{-1/2}$ are used. From (b), the solution is obtained by choosing the columns in the same directions as $\mathbf{V}_j^{\text{null}\dagger}\mathbf{H}_j^\dagger\mathbf{H}_j\mathbf{V}_j$ to maximize the trace-value as

$$\mathbf{S}_j=\mathbb{O}\left(\mathbf{V}_j^{\text{null}\dagger}\mathbf{H}_j^\dagger\mathbf{H}_j\mathbf{V}_j\mathbf{D}_{Vj}\mathbf{D}_{Vnj}\right)\tag{28}$$

$$\equiv\mathbb{O}\left(\mathbf{V}_j^{\text{null}\dagger}\mathbf{H}_j^\dagger\mathbf{H}_j\mathbf{V}_j\right),\tag{29}$$

where the equivalence can be considered due to the fact that $\mathbf{X}_j$, $\mathbf{Y}_j$ and $\mathbf{Z}_j$ are unknown, and thus, $\mathbf{S}_j$ can be independently and equivalently computed first. Further, letting $\mathbf{A}_j=\mathbf{V}_j^{\text{null}\dagger}\mathbf{H}_j^\dagger\mathbf{H}_j\mathbf{V}_j$, the cross-term below can be simplified as

$$\text{tr}\left(\mathbf{Y}_j^\dagger\mathbf{X}_j^\dagger\mathbf{V}_j^\dagger\mathbf{H}_j^\dagger\mathbf{H}_j\mathbf{V}_j^{\text{null}}\mathbf{S}_j\mathbf{Z}_j\right)=\text{tr}\left(\mathbf{Z}_j\mathbf{Y}_j^\dagger\mathbf{X}_j^\dagger\left(\mathbf{A}_j^\dagger\mathbf{A}_j\right)^{1/2}\right).$$

C. Getting $\mathbf{Z}_j$ and $\mathbf{X}_j$: an iterative approach

Further, from (26), squaring the terms on both sides yields the Cauchy Schwarz's inequality

$$\Re\text{tr}\left(\mathbf{Y}_j^\dagger\mathbf{X}_j^\dagger\mathbf{V}_j^\dagger\mathbf{H}_j^\dagger\mathbf{H}_j\mathbf{V}_j^{\text{null}}\mathbf{S}_j\mathbf{Z}_j\right)\tag{30a}$$

$$\leq\left\|\mathbf{H}_j\mathbf{V}_j\mathbf{X}_j\mathbf{Y}_j\right\|_F\left\|\mathbf{H}_j\mathbf{V}_j^{\text{null}}\mathbf{S}_j\mathbf{Z}_j\right\|_F,\tag{30b}$$

which suggests that equivalently, the above cross-term can be maximized to get the maximum harvested energy.

Since the matrices $\mathbf{Y}_j$ and $\mathbf{Z}_j$ can be relaxed to be diagonal as in Corollary 4, the matrix $\mathbf{Y}_j = \mathcal{D}\left(y_{j1}, \ldots y_{jd}\right)$ can be obtained from $\mathbf{Z}_j = \mathcal{D}\left(z_{j1}, \ldots z_{jd}\right)$ using the constraint in (24c) and (18) as

$$y_{ji} = +\sqrt{1 - z_{ji}^2}, \forall i = 1, \ldots, d, \tag{31}$$

satisfying the constraint in (24c). The remaining components of the CD decomposition can be computed as the solution of the following optimization problem as

$$\max_{\mathbf{Z}_j, \mathbf{X}_j} \Re\text{tr}\left(\mathbf{Y}_j^\dagger \mathbf{X}_j^\dagger \mathbf{V}_j^\dagger \mathbf{H}_j^\dagger \mathbf{H}_j \mathbf{V}_j^{\text{null}} \mathbf{S}_j \mathbf{Z}_j\right),$$

which is a non-convex problem due to the product of $\mathbf{Z}_j$ and $\mathbf{X}_j$. The efficient way to solve the problem is via an iterative method, where $\mathbf{X}_j$ and $\mathbf{Z}_j$ are solved alternately.

Given $\mathbf{Z}_j$ and $\mathbf{Y}_j$, the optimization problem above can be reduced to a convex problem as as

$$\max_{\mathbf{X}_j} \Re\text{tr}\left(\mathbf{Y}_j^\dagger \mathbf{X}_j^\dagger \mathbf{V}_j^\dagger \mathbf{H}_j^\dagger \mathbf{H}_j \mathbf{V}_j^{\text{null}} \mathbf{S}_j \mathbf{Z}_j\right) \tag{32a}$$

$$\text{subject to } \|\mathbf{X}_j\| \leq 1, \tag{32b}$$

where the spectral norm constraint above leads to the same constraint in (25e). The solution for $\mathbf{X}_j$ can be obtaining by choosing the same column directions as of $\mathbf{V}_j^\dagger \mathbf{H}_j^\dagger \mathbf{H}_j \mathbf{V}_j^{\text{null}} \mathbf{S}_j \mathbf{Z}_j \mathbf{Y}_j^\dagger$, i.e.,

$$\mathbf{X}_j = \mathbb{O}\left(\mathbf{V}_j^\dagger \mathbf{H}_j^\dagger \mathbf{H}_j \mathbf{V}_j^{\text{null}} \mathbf{S}_j \mathbf{Z}_j \mathbf{Y}_j^\dagger\right). \tag{33}$$

Note that the above $\mathbf{X}_j$ cannot be equivalently set to $\mathbb{O}\left(\mathbf{V}_j^\dagger \mathbf{H}_j^\dagger \mathbf{H}_j \mathbf{V}_j^{\text{null}} \mathbf{S}_j\right)$, since the above particular directions are important. Further, substituting $\mathbf{X}_j$ in the trace yields the following result.

Proposition 6. *With the above selection of $\mathbf{X}_j$, the trace-value is non-negative*

$$tr\left(\mathbf{Y}_j^\dagger \mathbf{X}_j^\dagger \mathbf{V}_j^\dagger \mathbf{H}_j^\dagger \mathbf{H}_j \mathbf{V}_j^{null} \mathbf{S}_j \mathbf{Z}_j\right) = tr\left[\left(\mathbf{B}_j^\dagger \mathbf{B}_j\right)^{1/2}\right] \geq 0,$$

where $\mathbf{B}_j = \mathbf{V}_j^\dagger \mathbf{H}_j^\dagger \mathbf{H}_j \mathbf{V}_j^{null} \mathbf{S}_j \mathbf{Z}_j \mathbf{Y}_j^\dagger = \left(\mathbf{A}_j^\dagger \mathbf{A}_j\right)^{1/2} \mathbf{Z}_j \mathbf{Y}_j^\dagger$, *and the equality occurs when* $z_j = 0$.

Next, given $\mathbf{Y}_j$, $\mathbf{X}_j$ and $z_j < z_j^{EH}$, the diagonal matrix $\mathbf{Z}_j$ can be updated as

$$\max_{\mathbf{Z}_j} \Re\text{tr}\left(\mathbf{Y}_j^\dagger \mathbf{X}_j^\dagger \mathbf{V}_j^\dagger \mathbf{H}_j^\dagger \mathbf{H}_j \mathbf{V}_j^{\text{null}} \mathbf{S}_j \mathbf{Z}_j\right) \tag{34a}$$

$$\text{subject to } \|\mathbf{Z}_j\|_F \leq \sqrt{z_j}, \tag{34b}$$

$$\mathbf{Z}_j \text{ is a diagonal matrix}, \tag{34c}$$

$$\mathbf{0} \preceq \mathbf{Z}_j \preceq \mathbf{I}, \tag{34d}$$

which is also a convex problem. We can equivalently recast the problem for $\mathbf{z}_j^T = [z_{j1}, \dots z_{jd}]$ as

$$\max_{\mathbf{z}_j} \mathbf{c}_j^T \mathbf{z}_j \tag{35a}$$

$$\text{subject to } \|\mathbf{z}_j\|_2 \leq \sqrt{z_j}, \tag{35b}$$

$$0 \leq z_{j,i} \leq 1, \forall i = 1, \dots, d, \tag{35c}$$

where the vector $\mathbf{c}_j = [c_{j1}, \dots, c_{jd}]$ and $c_{ji} = \left[\mathbf{Y}_j^\dagger \mathbf{X}_j^\dagger \mathbf{V}_j^\dagger \mathbf{H}_j^\dagger \mathbf{H}_j \mathbf{V}_j^{\text{null}} \mathbf{S}_j\right]_{i,i}, \forall i = 1, \dots, d$. The values $c_{ji}, \forall i$ are real and non-negative from the proposition 6. The solution of the above problem is given by choosing $\mathbf{z}_j$ equal to $\mathbf{c}_j$ and scaling it to satisfy the norm constraint. Thus, we write $z_{ji} = \min\left(\sqrt{z_j}\frac{c_{ji}}{\|\mathbf{c}_j\|}, 1\right)$, and normalize the resulting entries to satisfy $\sum_{i\in\mathcal{I}} z_{ji}^2 = z_j - (d - |\mathcal{I}|)$, where $\mathcal{I} = \{i : z_{ji} < 1\}$, i.e., $z_{ji} \leftarrow \frac{z_{ji}}{\sum_{i\in\mathcal{I}} z_{ji}^2}\sqrt{z_j - (d - |\mathcal{I}|)}, \forall i \in \mathcal{I}$.

D. Algorithm

Now, with all components obtained, the resulting balanced precoder can be computed via (25b). The summary of this procedure is given in Algorithm 1. If $z_j > z_j^{EH}$, we choose energy optimized precoder as the balanced precoder $\mathbf{V}_j^{BAL} = \mathbf{V}_j^{EH}$. Regarding the convergence, it can be seen that since both $\mathbf{Z}_j$ and $\mathbf{X}_j$ maximize the same linear objective, thus convergence is guaranteed with a global optimum value. Regarding the number of iterations, we observe via simulations that it takes only a few (4-8) iterations to converge.

E. Getting $\mathbf{Z}_j$ and $\mathbf{X}_j$: a non-iterative approach

Here, we present a suboptimal non-iterative method to compute $\mathbf{X}_j$ and $\mathbf{Z}_j$. This method is based on upper bound in the equation (26). In (26), applying the max-operator on both sides

Algorithm 1 Iterative CD decomposition procedure.

Input: $\mathbf{H}_j$, $\mathbf{V}_j$ and z_j.

Output: $\mathbf{V}_j^{BAL}$.

1: **if** $z_j > z_j^{EH}$ **then**
2: Return $\mathbf{V}_j^{BAL} = \mathbf{V}_j^{EH}$.
3: **else**
4: Compute $\mathbf{S}_j = \mathbb{O}\left(\mathbf{V}_j^{\text{null}\dagger}\mathbf{H}_j^{\dagger}\mathbf{H}_j\mathbf{V}_j\right)$.
5: Initialize $\mathbf{Z}_j = \sqrt{\frac{z_j}{d}}\mathbf{I}$ and $\mathbf{Y}_j$ by (31).
6: Solve (32a) to get $\mathbf{X}_j$.
7: Solve (34a) to get $\mathbf{Z}_j$.
8: Get $\mathbf{Y}_j$ by (31).
9: Go to step 6 until convergence.
10: Return $\mathbf{V}_j^{BAL}$ via (25b).
11: **end if**

yields

$$\begin{aligned}&\max_{\mathbf{S}_j,\mathbf{Z}_j,\mathbf{X}_j,\mathbf{Y}_j} \left\|\mathbf{H}_j\left(\mathbf{V}_j\mathbf{X}_j\mathbf{Y}_j + \mathbf{V}_j^{\text{null}}\mathbf{S}_j\mathbf{Z}_j\right)\right\|_F \\ &\leq \max_{\mathbf{X}_j,\mathbf{Y}_j} \left\|\mathbf{H}_j\mathbf{V}_j\mathbf{X}_j\mathbf{Y}_j\right\|_F + \max_{\mathbf{S}_j,\mathbf{Z}_j} \left\|\mathbf{H}_j\mathbf{V}_j^{\text{null}}\mathbf{S}_j\mathbf{Z}_j\right\|_F, \end{aligned} \tag{36}$$

Thus, for a lower complexity solution, we solve the right hand side get the components for the balanced precoding.

Given $z_j < z_j^{EH}$, the matrix $\mathbf{Z}_j$ can be obtained to maximize the harvested power as

$$\mathbf{Z}_j = \arg\max_{\mathbf{Z}_j \forall j} \left\|\mathbf{H}_j\mathbf{V}_j^{\text{null}}\mathbf{S}_j\mathbf{Z}_j\right\|_F^2 \tag{37}$$

$$\text{subject to (34b), (34c), (34d).}$$

The above problem can be simplified as

$$\max_{0\leq z_{ji}\leq 1,\forall i} \sum_i z_{ji}^2 f_{ji} \tag{38a}$$

$$\text{subject to } \sum_i z_{ji}^2 \leq z_j, \tag{38b}$$

where the values $f_{ji} = \left[\mathbf{S}_j^{\dagger}\mathbf{V}_j^{\text{null}\dagger}\mathbf{H}_j^{\dagger}\mathbf{H}_j\mathbf{V}_j^{\text{null}}\mathbf{S}_j\right]_{i,i}, \forall i = 1,\ldots,d$ are real and non-negative. For the solution of the above optimization, we write

$$z_{ji}^2 = \min\left(z_j\frac{f_{ji}}{\sum_i f_{ji}}, 1\right), \forall i = 1,\ldots,d, \tag{39}$$

and normalize the resulting entries ($\mathcal{I} = \{i : z_{ji} < 1\}$) to satisfy $\sum_{i\in\mathcal{I}} z_{ji}^2 = z_j - (d - |\mathcal{I}|)$.

Next, the matrix $\mathbf{Y}_j$ can be computed using (31). Further, the matrix $\mathbf{X}_j$ can be chosen as

$$\mathbf{X}_j = \arg\max_{\|\mathbf{X}_j\|\leq 1} \|\mathbf{H}_j\mathbf{V}_j\mathbf{X}_j\mathbf{Y}_j\|_F^2 \tag{40}$$

$$= \mathbb{O}\left(\mathbf{V}_j^{\dagger}\mathbf{H}_j^{\dagger}\mathbf{H}_j\mathbf{V}_j\mathbf{Y}_j^{-1}\right). \tag{41}$$

The resulting j^{th} precoder $\mathbf{V}_j^{BAL}$ can be given via (25b).

F. Computational complexity

The product $\mathbf{H}_j^{\dagger}\mathbf{H}_j$ and its EVD need $\mathcal{O}(M^2NK)$ and $\mathcal{O}(M^3)$ operations. For $\mathbf{S}_j$, the product and $\mathbb{O}(\cdot)$ need $\mathcal{O}(NK\cdot M(M-d) + NKd\cdot M + NK(M-d)\cdot M) = \mathcal{O}(NKM^2)$ and $\mathcal{O}(d^2\cdot(M-d)+d^3) = \mathcal{O}(Md^2)$. The rest of operations are below $\mathcal{O}(Md^3)$ or $\mathcal{O}(M^3)$. Thus, if $M = N$, Algorithm 1 has $\mathcal{O}(M^3K + Md^2N_I) \approx \mathcal{O}(M^3K)$ computational complexity, where the number of iterations N_I for convergence are few (4-8), i.e. $N_I \ll \frac{KM^2}{d^2}$. Similarly, non-iterative process has the same complexity.

G. Bounds on the harvesting Energy

Note that not any trivial balanced precoding can guarantee the better harvested energy. For the balanced precoding, the following bounds can be obtained.

Lemma 7. *Given balanced precoding $\left\{\mathbf{V}_k^{BAL}, \forall k\right\}$ for the channel $\{\mathbf{H}_{kj}, \forall k, j\}$ with IA precoders $\{\mathbf{V}_k, \forall k\}$, the total harvested energy can be bounded as*

$$\zeta\sum_{j=1}^{K}\frac{P_j}{d}\left[\|\mathbf{H}_j\mathbf{V}_j\|_F^2\left(1-\frac{z_j}{d}\right) + \left\|\mathbf{H}_j\mathbf{V}_j^n\right\|_F^2\left(\frac{z_j}{d}\right)\right] \tag{42a}$$

$$\leq \sum_{k=1}^{K} Q_k(\bar{\rho}_k, \mathbf{V}_k^{BAL}) \leq \zeta\sum_{j=1}^{K} P_j\lambda_{j1}. \tag{42b}$$

Proof: Proof is given in Appendix-B. ■

The above result shows an improvement over (11), i.e., the balanced precoding promises the better harvested energy than that achieved using just perfect IA precoders. With the balanced precoding, the resultant rate loss can be obtained from the upper bound in the Lemma 5.

With $\bar{\rho}_k = \bar{\rho}, \forall k$ and with $\mathcal{CN}(0,1)$ entries in $\mathbf{H}_{kj}$, performing the exception on both the sides in the above equation gives

$$\zeta \bar{\rho} KN \sum_j P_j \approx \sum_{k=1}^{K} \mathbb{E}\left\{Q_k(\bar{\rho})\right\} \tag{43a}$$

$$\leq \zeta \bar{\rho} KNd \left(\frac{KN+d}{KNd+1}\right)^{2/3} \sum_{j=1}^{K} P_j, \tag{43b}$$

where the left approximation is obtained assuming $\mathbb{E}\left\|\mathbf{H}_j \mathbf{V}_j^{BAL}\right\|_F^2 \approx \bar{\rho} KNd$, and the right inequality is given by $\mathbb{E}\left\{\lambda_{j1}\right\} = \bar{\rho} KNd \left(\frac{KN+d}{KNd+1}\right)^{2/3}$ [47].

V. Energy Harvesting with Feedback

In the above formulation for EH, perfect IA precoder has been employed, which is not the case in practice. In practice, to avail the precoder at the transmitter side, either CSI or precoder is fed back in quantized or analog form. In this section, considering precoder feedback, the sum rate and energy harvesting terms are analyzed. Recall that the trade off between these is characterized by the chordal distance. In literature, it has been demonstrated that chordal distance is an integral part of the feedback systems. Therefore, in the following analog precoder feedback scheme is provided, followed by limited precoder feedback.

A. Analog Feedback

In analog feedback, after the estimation of the reverse links, full ($M \times d$) precoder is sent back using analog transmission [27]. In orthogonal transmission case, destinations transmit simultaneously in Kd time slots respectively. After receiving the noisy precoder information at the sources, the orthogonalization of the MMSE estimate is performed to obtain the final precoder estimate.

From the results in [27], it can be observed that for lower feedback SNR, the chordal distance remains constant and so, the sum rate loss increases with SNR (see Lemma 5). On the other hand, for medium to high SNR case, the chordal distance decreases inversely proportional to SNR, which keeps the rate loss constant for this SNR range. In IA scenarios, the medium to high SNR regime is of more importance. In conjunction with energy harvesting, one can note that the chordal distance dynamically changes according to the feedback SNR selected at the destinations. The conclusion of this result is that analog feedback also helps in increasing energy

efficiency while maintaining linear sum rate scaling. To get the desired energy in harvesting, only the splitting factor needs to be selected using the results in the previous section.

For perfect CSI, given the RLUB ($\Delta R_{\max}$), CD value can be obtained as

$$z = \frac{d(M-d)}{(K-1)M}\left(\frac{P}{\sigma^2}\right)^{-1}\left(2^{\frac{\Delta R_{\max}}{d}}-1\right), \tag{44}$$

from Lemma 5.

B. Quantized Feedback

Let the vector $\mathbf{b} = [b_1, b_2, \ldots, b_K]^T$ denote the number of feedback bits allocated for each user. The corresponding precoder quantization codebook of size 2^{b_k} is given as $\mathcal{C}(b_k) = \{\mathbf{C}_1(b_k), \ldots, \mathbf{C}_{2^{b_k}}(b_k)\}$ where each entry $\mathbf{C}_i(b_k)$ is an $M \times d$ orthogonal matrix such that $\mathbf{C}_i(b_k)^\dagger \mathbf{C}_i(b_k) = \mathbf{I}_d$. The codebook $\mathcal{C}(b_k)$ for each b_k is considered to be known to all the transmitters and receivers. The precoder matrix index (PMI) vector is denoted as $\mathbf{q} = [q_1, \ldots, q_K]^T$ with each q_k representing an index from the codebook $\mathcal{C}(b_k)$, i.e. $1 \leq q_k \leq 2^{b_k}$, $\forall k$.

In the conventional method, when the perfect IA precoders are available, each of the precoders is quantized using the chordal distance metric. Let $\mathbf{q}_{CD}$ denote the PMI vector obtained using quantization based on chordal distance. The k^{th} index of $\mathbf{q}_{CD}$ is obtained as

$$q_{CD,k} = \arg\min_{\mathbf{C}_i \in \mathcal{C}} d_c^2(\mathbf{V}_k, \mathbf{C}_i), \tag{45}$$

where $q_{CD,k}$ is the index of the closest codebook entry. This technique incurs a low computational complexity. Improved precoder feedback schemes can be seen in [28], [29] which suggest that the sum rate can be improved for the same number of quantization bits. The main point is to observe that the limited feedback can increase the harvested energy since chordal distance is non-zero. Note that the resultant chordal distance of quantized precoders varies inversely proportional to the codebook size, i.e., as codebook size increases EH decreases and sum rate increases. Therefore, given the codebook, the chordal distance can be fixed as

$$z = \mathbb{E}d_c^2(\mathbf{V}_k, \mathbf{C}_i) < 2^{-\frac{B}{d(M-d)}}, \tag{46}$$

and splitting ratio can be varied to get the desired harvested energy.

Remark (SNR shift): For $z = 0$, the splitting causes the noise variance to change from σ^2 to σ_{ID}^2, which causes the $\left(\frac{\sigma_{ID}^2}{\sigma^2}\right)_{dB} = \left(1 + \frac{\delta^2}{\rho_k \sigma^2}\right)_{dB}$ shift in SNR without loosing linear sum rate scaling. It shows that the splitting factor can be obtained to maintain linear rate scaling with a given SNR shift or a given constant rate loss. For example, to get only 3 dB loss in sum rates, $1 + \frac{\delta^2}{\rho_k \sigma^2} = 2$ or $\rho_k = 1 - \bar{\rho}_k = \frac{\delta^2}{\sigma^2}$.

VI. Simulation Results

A. Simulation settings

The value of essential variables are given as follows: $\rho_k = \zeta = 0.5, \forall k$, $P_k = P$ and $z_j = z$. We consider two IA-feasible systems (a) $(4 \times 4, 2)^3$ and (b) $(5 \times 5, 2)^3$. Each entry of $\mathbf{H}_{kj}$ is assumed to be distributed as $\mathcal{CN}(0, 1)$. For balanced precoding, the iterative process (ICD) is run for a maximum of 6 iterations. We assume for all j, $z_j = z < \min_j z_j^{EH}$. In the following figures, we compare different precoding strategies given below.

- (RAND) Random full rank precoder with orthogonal columns;
- (MAX-EH) Harvested energy maximizing precoder;
- (SSIA) Balanced Precoders from subspace IA method with $z = 0, 0.1, 0.8$;
- (MMSEIA) Balanced precoder from MMSE based IA algorithm [45] with $z = 0, 0.1, 0.8$;
- (PQFB) Precoder obtained from quantized feedback from a given codebook of size 6 bits [45];
- Precoder acquired via analog precoder feedback (PAFB) [27] , and via analog CSI feedback (CSIAFB) [48] with similar feedback transmission power as the forward one, $P_f = P$.

B. Rate-energy region plots

Given the precoders $\{\mathbf{V}_k, \forall k\}$, the rate-energy region can be written as [49], [50], $\mathcal{C} =$

$$\bigcup_{\boldsymbol{\rho}} \left\{ (R, Q) : R \leq \sum_{k=1}^{K} R_k \left(\rho_k, \mathbf{V}_k\right), Q \leq \sum_{k=1}^{K} Q_k \left(\rho_k, \mathbf{V}_k\right) \right\}, \tag{47}$$

where $\boldsymbol{\rho} = [\rho_1, \ldots, \rho_K]$ is a vector of K splitting factors. For a splitting noise variance $\delta^2 = 0.1$, assuming $\rho_k = \rho, \forall k$ varying ρ from 0 to 1, the parametric plots are drawn to illustrate rate-energy regions [49], [50].

Figure 1 shows the sum rate versus the total harvested energy plot for three types of precoders, viz., MSE-IA, MAX-EH and MSE-IA with balanced precoding. It can be seen that MSE-IA region has higher sum rates and lower energies, while the region for MAX-EH precoders has less sum rates and higher energies. These plots represent two extreme ends of rate and energy achievabililty. Next, for the balanced precoding with iterative method, it can be observed that as z increases, the rate decreases and energy increases, when $z < \min_j z_j^{EH}$. When $z > \min_j z_j^{EH}$, both rate and energy achieved are lower. Therefore, for the case of $z > \min_j z_j^{EH}$, it is better to employ MAX-EH precoder than IA-precoder.

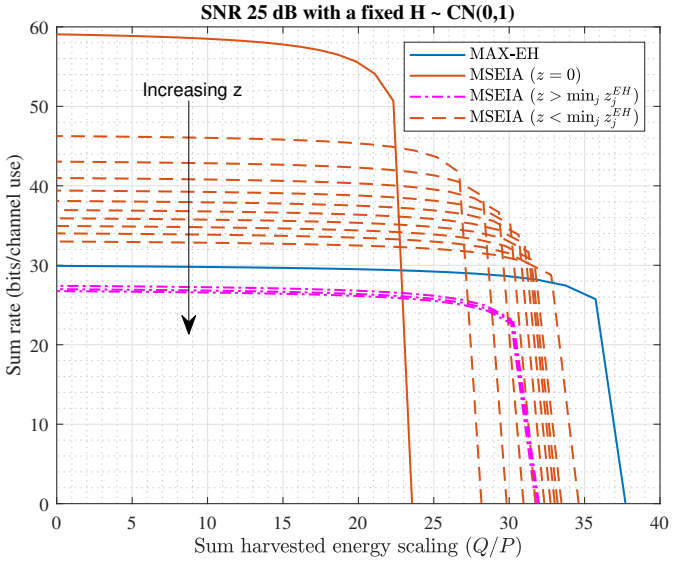

Figure 1. Rate-energy plot for $(5 \times 5, 2)^3$ system for iterative CD decomposition.

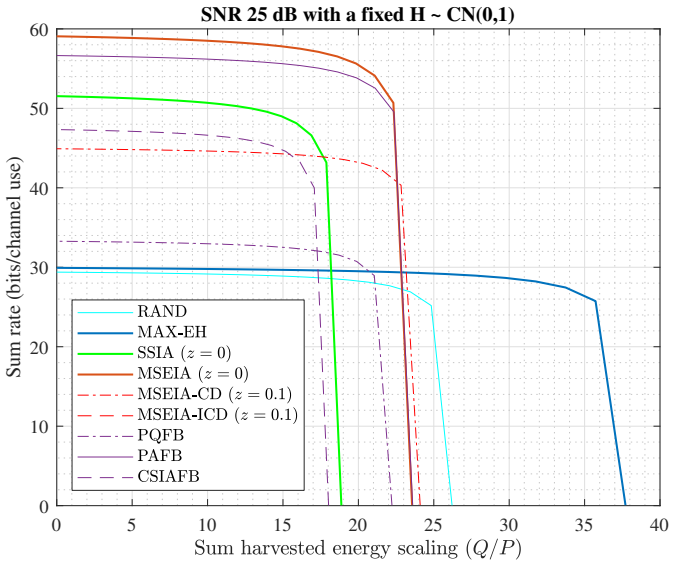

Figure 2. Rate-energy plot for $(5 \times 5, 2)^3$ system for different precoding methods.

Figure 2 compares the same rate-energy region for different precoding schemes. The following points can be concluded from the figure.

- $\mathcal{C}_{\text{RAND}} \subset \mathcal{C}_{\text{MAX-EH}}$ and $\mathcal{C}_{\text{RAND}} \subset \mathcal{C}_{\text{MSEIA-ICD}}$: Random precoders have worst rates.
- $\mathcal{C}_{\text{SSIA}} \subset \mathcal{C}_{\text{MSEIA}}$: Among IA-methods, MSE based methods are better suited for both rate and energy optimization.

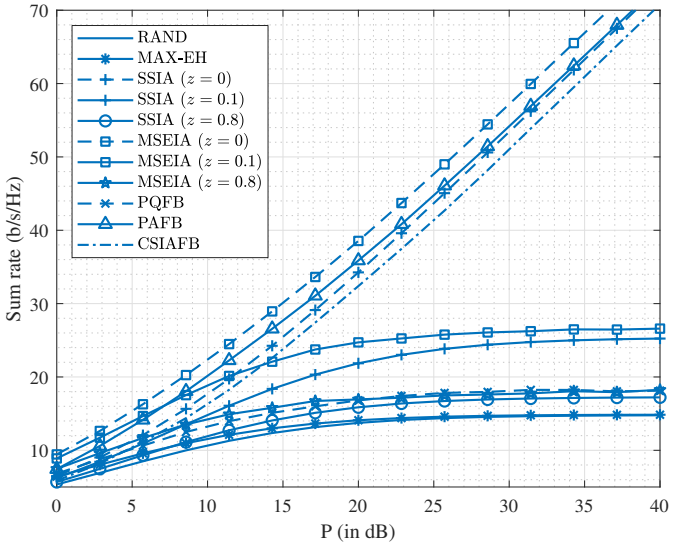

Figure 3. Sum rates versus SNR with $(4 \times 4, 2)^3$system.

- $\mathcal{C}_{\text{CSIAFB}} \subset \mathcal{C}_{\text{PAFB}}$ and $\mathcal{C}_{\text{PQFB}} \subset \mathcal{C}_{\text{PAFB}}$: Analog precoder feedback is better than both analog CSI feedback and precoder quantizated feedback.
- $\mathcal{C}_{\text{MSEIA-CD}} \subset \mathcal{C}_{\text{MSEIA-ICD}}$: Iterative balanced precoding method provides better rate and energy than that via non-iterative one. Therefore, in the following, iterative method based precoding is considered for comparison.

C. Sum Rate and harvested energy versus SNRs

Figure 3-4 illustrate the sum rates with respect to SNR for $(4 \times 4, 2)^3$ and $(5 \times 5, 2)^3$ systems, respectively. It can be observed that both SSIA and MSEIA ($z = 0$) achieve linear sum rate scaling with SNR, while with $z > 0$, saturating sum rates are obtained at high SNR. As compared to $(4 \times 4, 2)^3$ system, the saturation in sum rates starts at higher SNR for $(5 \times 5, 2)^3$ system, since more spatial dimensions are available in $(5 \times 5, 2)^3$ to grant diversity gains. For limited feedback with 8 quantization bits per precoder, similar rate losses can be seen due to saturation, because to keep the rate loss constant number of bits need to be scaled proportional to SNR [45]. For analog feedback (AFB) schemes (CSIAFB and PAFB), a constant rate loss can be observed at high SNR regime, yielding the better performance than quantization schemes. Figure 4 plots the similar trend for $(5 \times 5, 2)^3$ system, except that higher sum rates are achieved due to more spatial dimensions.

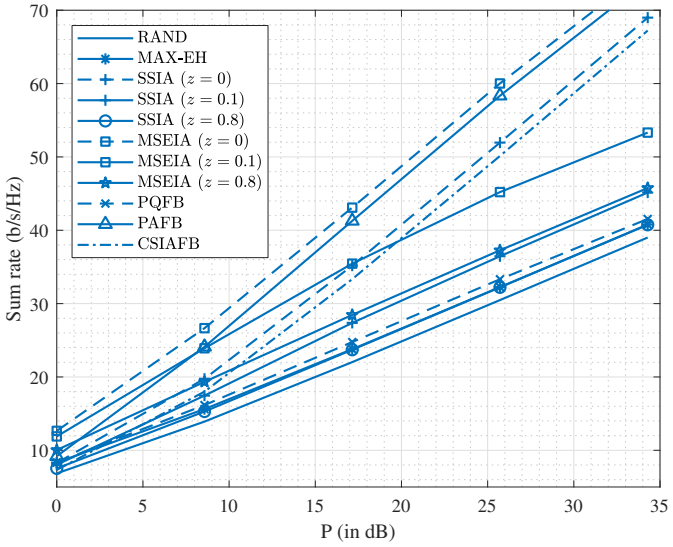

Figure 4. Sum rates versus SNR with $(5 \times 5, 2)^3$ system.

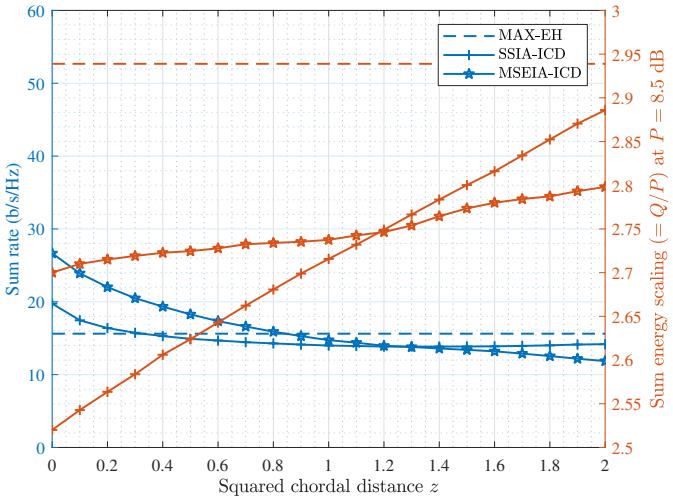

Figure 5. Figure illustrates both the sum rate and sum harvested power variations versus chordal distance for $(5 \times 5, 2)^3$ at 25 dB SNR.

D. Rate-Energy performance versus chordal distance

Figure 5 plots the sum rate (left-axis) and the harvested energy (right-axis) versus the squared chordal distance $z = d_c^2\left(\mathbf{V}_j, \mathbf{V}_j^{BAL}\right), \forall j$ required for the balanced precoding with MSE-IA and SS-IA. It can be seen that the sum rate decreases in a logarithmic manner as z increases. This behavior has been analyzed in the Lemma 21 for rate-loss upper bound. On the other hand, harvested energy is increased, if z is increased. Upto a certain value of z (say z_{th}), MSE-IA

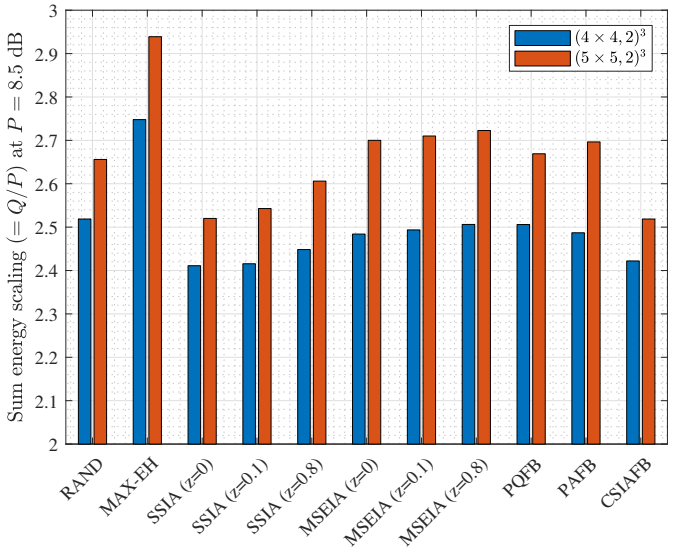

Figure 6. Figure showing the sum harvested power scaling for different precoding methods for $(4 \times 4, 2)^3$ and $(5 \times 5, 2)^3$ systems at 25 dB SNR.

provides higher energies than that with SS-IA. When $z > z_{th}$, SS-IA yields better energy output. Regarding the sum rate intersection between MAX-EH and MSE-IA (or SS-IA), it is the point when $z = \min_j z_j^{EH}$. When $z > \min_j z_j^{EH}$, both rate and energy are lower than that of MAX-EH. Thus, it is better to consider MAX-EH precoder beyond this intersection. Note that the earlier intersection of SS-IA than MSE-IA is due to the fact that MSE-IA provides better sum rates than SS-IA in general.

E. Energy scaling with SNRs

The respective harvested energy scaling (with respect to transmit power (P)) is illustrated in Figure 6 for different precoding strategies. Max-EH precoding provides maximum scaling. MSE-IA methods provide better scaling than SS-IA based ones. Also, for rate-energy balanced precoding, increasing the chordal distance shows increase in scaling. This result is also depicted in Figure 5, which shows the sum rate and EH scaling variations with respect to chordal distance. It can be seen that the energy scales linearly with chordal distance. The most efficient method is PAFB, where the chordal distance is selected automatically inversely proportional to feedback SNR. It suggests to choose the chordal distance carefully based on SNR and the required harvested energy constraint.

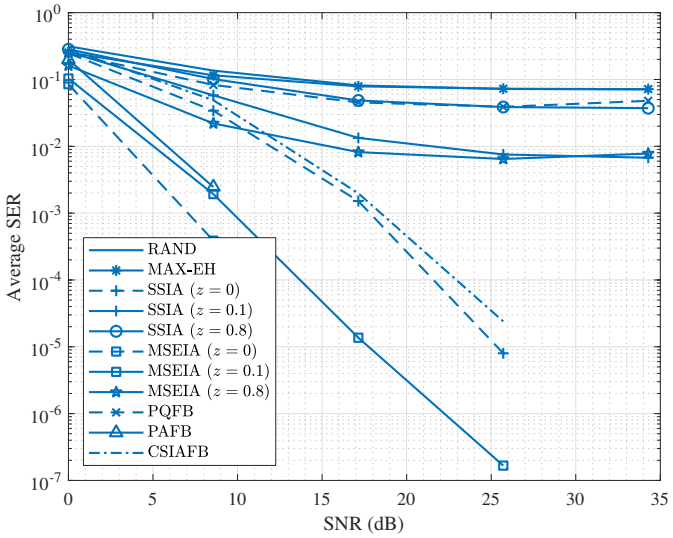

Figure 7. Figure depicts the average QPSK symbol error rate (SER) with respect to SNR for $(5 \times 5, 2)^3$.

F. SER plots

Figure 7 depicts the average SER plots with QPSK modulation for $(5 \times 5, 2)^3$. It can be seen that perfect IA precoders ($z = 0$) achieve the minimum SER, while with $z = 0.1, 0.8$, the SER saturates. For quantization based methods, the SER can be seen to be higher. Among the feedback schemes, APFB methods can be seen to provide a significantly better SER, close to perfect MSE-IA scheme. More importantly, APFB methods also yield linear sum rate scaling and EH scaling approximately to MSE-IA ($z = 0.1$), which shows the effectiveness of APFB schemes.

VII. Conclusion

In this paper, we have provided a low-complexity systematic balanced precoding method towards getting the improved trade-off between sum rate and harvested energy. First, the precoder that achieves maximum harvested energy has been computed. Thereafter, utilizing the CD decomposition, we have systematically derived and analyzed the proposed precoder for SWIPT trade-off. The lower and upper bounds on harvested energy for this construction have been obtained. Due to the dependence on CD, the relations to the analog and limited feedback schemes have been discussed. Simulation results show that MSE based methods are better for SWIPT than subspace alignment method or leakage minimization algorithm. Among feedback

schemes, APFB provides improved sum rates without loosing the linear scaling (with SNR) as well as improved harvested energy.

APPENDICES

A. Proof of CD decomposition

Consider two $M \times d$ orthonormal matrices $\mathbf{V}, \hat{\mathbf{V}}$ such that $\mathbf{V}^\dagger\mathbf{V} = \hat{\mathbf{V}}^\dagger\hat{\mathbf{V}} = \mathbf{I}_d$. Its left null space of size $M \times M-d$ can be represented as $\hat{\mathbf{V}}_j^{\text{null}} = \text{null}(\hat{\mathbf{V}}_j)$. Then, we can write

$$\mathbf{V} = \hat{\mathbf{V}}\hat{\mathbf{V}}^\dagger\mathbf{V} + \left(\mathbf{I}_M - \hat{\mathbf{V}}\hat{\mathbf{V}}^\dagger\right)\mathbf{V} \tag{48}$$

$$= \hat{\mathbf{V}}\underbrace{\hat{\mathbf{V}}^\dagger\mathbf{V}}_{=\mathbf{XY}} + \hat{\mathbf{V}}^{\text{null}}\underbrace{\hat{\mathbf{V}}^{\text{null}\dagger}\mathbf{V}}_{=\mathbf{SZ}} \tag{49}$$

where the last equation is obtained by the QR-decomposition such that $\mathbf{X}$ and $\mathbf{S}$ are $d \times d$ and $M-d \times d$ orthonormal matrices respectively. It verifies $d_c^2(\mathbf{V}, \hat{\mathbf{V}}) = d - \|\hat{\mathbf{V}}^\dagger\mathbf{V}\|_F^2 = d - \text{tr}(\mathbf{Y}^\dagger\mathbf{Y}) = \text{tr}(\mathbf{Z}^\dagger\mathbf{Z})$. Note that $\mathbf{XY} \in \mathbb{C}^{d\times d}$ is independent of $\hat{\mathbf{V}} \in \mathbb{C}^{M\times d}$, since $\mathbf{XY}$ is a projection to a lower dimension space. Also, the factors $\mathbf{X}$ and $\mathbf{Y}$ are independent, since $\mathbf{X}$ represents the basis of $\hat{\mathbf{V}}^\dagger\mathbf{V}$ and the basis are not unique. Using similar facts, the matrices $\mathbf{S}$ and $\mathbf{Z}$ are also independent. For more details, visit [24].

B. Proof of Lemma 7

Proof: The inequality in the upper bound comes from (13) as $\frac{1}{d}\sum_{i=1}^{d}\left\|\mathbf{H}_j\mathbf{V}_j^{BAL}\right\|_F^2 \leq \frac{1}{d}\sum_{i=1}^{d}\lambda_{ji} \leq \lambda_{j1}, \forall j$, where the equality occurs when $z_j = z_j^{EH}, \forall j$, and the second inequality is due to the fact that the average of d-values is less than the the maximum of them.

The inequality of the lower bound can be derived from the CD decomposition, where the equality occurs, when $z_j = 0, \forall j$. For the proposed balanced precoder with the optimum values of $\mathbf{X}_j^*, \mathbf{Y}_j^*, \mathbf{S}_j^*$ and $\mathbf{Z}_j^*$, we can write

$$\begin{aligned}
&\left\|\mathbf{H}_j\mathbf{V}_j^{BAL}\right\|_F^2 \\
&= \left\|\mathbf{H}_j\mathbf{V}_j\mathbf{X}_j^*\mathbf{Y}_j^* + \mathbf{H}_j\mathbf{V}_j^{\text{null}}\mathbf{S}_j^*\mathbf{Z}_j^*\right\|_F^2 \\
&\overset{(a)}{\geq} \left\|\mathbf{H}_j\mathbf{V}_j\mathbf{X}_j^*\sqrt{1-\frac{z_j}{d}} + \mathbf{H}_j\mathbf{V}_j^{\text{null}}\mathbf{S}_j^*\sqrt{\frac{z_j}{d}}\right\|_F^2 \\
&\overset{(b)}{\geq} \left\|\mathbf{H}_j\mathbf{V}_j\mathbf{X}_j^*\right\|_F^2\left(1-\frac{z_j}{d}\right) + \left\|\mathbf{H}_j\mathbf{V}_j^{\text{null}}\mathbf{S}_j^*\right\|_F^2\left(\frac{z_j}{d}\right) \\
&\overset{(c)}{\geq} \left\|\mathbf{H}_j\mathbf{V}_j\right\|_F^2\left(1-\frac{z_j}{d}\right) + \left\|\mathbf{H}_j\mathbf{V}_j^{\text{n}}\right\|_F^2\left(\frac{z_j}{d}\right),
\end{aligned}$$

where in (a), the maximum value of norm is upper bounded by trivial selection $\mathbf{Z}_j = \mathbf{I}\sqrt{1-\frac{z_j}{d}}$; in (b), we employ the fact that the trace value in the above norm-expansion is non-negative for the proposed scheme, as mentioned in the proposition 6; and in (c), the specific d-dimensional null space $\left(\mathbf{V}_j^{\text{null}}\mathbf{S}_j^*\right)$ can be replaced with any other d-dimensional null space $\mathbf{V}_j^{\text{n}} \in \mathcal{G}_{M,d}$ of $\mathbf{V}_j$. ■

REFERENCES

[1] N. Zhao, F. R. Yu, and V. C. M. Leung, "Wireless energy harvesting in interference alignment networks," *IEEE Communications Magazine*, vol. 53, no. 6, pp. 72–78, 2015.

[2] Z. G. Wan, Y. K. Tan, and C. Yuen, "Review on energy harvesting and energy management for sustainable wireless sensor networks," in *IEEE 13th International Conference on Communication Technology*, Sep. 2011, pp. 362–367.

[3] R. Prasad, S. Devasenapathy, V. Rao, and J. Vazifehdan, "Reincarnation in the ambiance: Devices and networks with energy harvesting," *IEEE Communications Surveys and Tutorials*, vol. 16, no. 1, pp. 195–213, 2014.

[4] C. Valenta and G. Durgin, "Harvesting wireless power: Survey of energy-harvester conversion efficiency in far-field, wireless power transfer systems," *IEEE Microwave Magazine*, vol. 15, no. 4, pp. 108–120, 2014.

[5] R. Vyas, B. Cook, Y. Kawahara, and M. Tentzeris, "E-WEHP: A batteryless embedded sensor-platform wirelessly powered from ambient digital-TV signals," *IEEE Transactions on Microwave Theory and Techniques*, vol. 61, no. 6, pp. 2491–2505, 2013.

[6] I. Krikidis, S. Timotheou, S. Nikolaou, G. Zheng, D. Ng, and R. Schober, "Simultaneous wireless information and power transfer in modern communication systems," *IEEE Communications Magazine*, vol. 52, no. 11, pp. 104–110, 2014.

[7] M. Khandaker and K.-K. Wong, "Swipt in MISO multicasting systems," *IEEE Wireless Communications Letters*, vol. 3, no. 3, pp. 277–280, 2014.

[8] Q. Shi, L. Liu, W. Xu, and R. Zhang, "Joint transmit beamforming and receive power splitting for MISO SWIPT systems," *IEEE Transactions on Wireless Communications*, vol. 13, no. 6, pp. 3269–3280, 2014.

[9] Q. Shi, W. Xu, T.-H. Chang, Y. Wang, and E. Song, "Joint beamforming and power splitting for MISO interference channel with SWIPT: An SOCP relaxation and decentralized algorithm," *IEEE Transactions on Signal Processing*, vol. 62, no. 23, pp. 6194–6208, 2014.

[10] B. Xu, Y. Zhu, and R. Zhang, "Optimal power allocation for a two-link interference channel with SWIPT," in *Sixth International Conference on Wireless Communications and Signal Processing (WCSP)*, Oct 2014, pp. 1–5.

[11] Z. Zong, H. Feng, F. Yu, N. Zhao, T. Yang, and B. Hu, "Optimal transceiver design for SWIPT in K-user MIMO interference channels," *IEEE Transactions on Wireless Communications*, vol. 15, no. 1, pp. 430–445, 2016.

[12] L. R. Varshney, "Transporting information and energy simultaneously," in *IEEE International Symposium on Information Theory*, July 2008, pp. 1612–1616.

[13] P. Grover and A. Sahai, "Shannon meets Tesla: Wireless information and power transfer," in *IEEE International Symposium on Information Theory*, June 2010, pp. 2363–2367.

[14] R. Zhang and C. Ho, "MIMO broadcasting for simultaneous wireless information and power transfer," *IEEE Transactions on Wireless Communications*, vol. 12, no. 5, pp. 1989–2001, 2013.

[15] L. Liu, R. Zhang, and K.-C. Chua, "Wireless information and power transfer: A dynamic power splitting approach," *IEEE Transactions on Communications*, vol. 61, no. 9, pp. 3990–4001, 2013.

[16] X. Chen, C. Yuen, and Z. Zhang, "Wireless energy and information transfer tradeoff for limited-feedback multiantenna systems with energy beamforming," *IEEE Transactions on Vehicular Technology*, vol. 63, no. 1, pp. 407–412, 2014.

[17] V. Cadambe and S. Jafar, "Interference alignment and degrees of freedom of the K-user interference channel," *IEEE Transactions on Information Theory*, vol. 54, no. 8, pp. 3425–3441, 2008.

[18] N. Garg and G. Sharma, "Sum rate of k-user mimo interference channel for finite constellation inputs with interference alignment," in *National Conference on Communication (NCC)*, March 2016, pp. 1–4.

[19] T. Xu and X.-g. Xia, "A diversity analysis for distributed interference alignment using the max-SINR algorithm," *IEEE Transactions on Information Theory*, vol. 60, no. 3, pp. 1857–1868, 2014.

[20] S. M. Razavi and T. Ratnarajah, "Adaptive LS and MMSE-Based Beamformer Design for Multiuser MIMO Interference Channels," *IEEE Transactions on Vehicular Technology*, vol. 65, no. 1, pp. 132–144, Jan 2016.

[21] N. Garg and G. Sharma, "Interference alignment in cellular system with multiple d2d networks," in *International Conference on Signal Processing and Communications (SPCOM)*, June 2016, pp. 1–4.

[22] S. W. Peters and R. W. Heath Jr., "Interference alignment via alternating minimization," in *IEEE International Conference on Acoustics, Speech and Signal Processing (ICASSP)*, 2009, pp. 2445–2448.

[23] K. Anand, E. Gunawan, and Y. Guan, "Beamformer design for the MIMO interference channels under limited channel feedback," *IEEE Transactions on Communications*, vol. 61, no. 8, pp. 3246–3258, 2013.

[24] N. Ravindran and N. Jindal, "Limited feedback-based block diagonalization for the MIMO broadcast channel," *IEEE Journal on Selected Areas in Communications*, vol. 26, no. 8, pp. 1473–1482, 2008.

[25] N. Jindal, "MIMO broadcast channels with finite-rate feedback," *IEEE Transactions on Information Theory*, vol. 52, no. 11, pp. 5045–5060, 2006.

[26] R. Krishnamachari and M. Varanasi, "Interference alignment under limited feedback for MIMO interference channels," *IEEE Transactions on Signal Processing*, vol. 61, no. 99, pp. 3908–3917, 2013.

[27] N. Garg and G. Sharma, "Analog precoder feedback schemes with interference alignment," *IEEE Transactions on Wireless Communications*, vol. 17, no. 8, pp. 5382–5396, Aug 2018.

[28] ——, "Precoder quantization for interference alignment with limited feedback," in *IEEE Wireless Communications & Networking Conference (WCNC)*, 2015, pp. 281–286.

[29] N. Garg and G. Sharma, "A quantization method for precoder feedback in interference channel," in *International Conference on Signal Processing and Communications (SPCOM)*, June 2016, pp. 1–5.

[30] X. Chen and C. Yuen, "Performance analysis and optimization for interference alignment over MIMO interference channels with limited feedback," *IEEE Transactions on Signal Processing*, vol. 62, no. 7, pp. 1785–1795, 2014.

[31] J. Park and B. Clerckx, "Transmission strategies for joint wireless information and energy transfer in a two-user mimo interference channel," in *IEEE International Conference on Communications Workshops (ICC)*, June 2013, pp. 591–595.

[32] S. Lee, L. Liu, and R. Zhang, "Collaborative wireless energy and information transfer in interference channel," *IEEE Transactions on Wireless Communications*, vol. 14, no. 1, pp. 545–557, Jan 2015.

[33] S. Timotheou, I. Krikidis, and B. Ottersten, "MISO interference channel with QoS and RF energy harvesting constraints," in *IEEE International Conference on Communications (ICC)*, June 2013, pp. 4191–4196.

[34] N. Zhao, F. R. Yu, and H. Sun, "Adaptive energy-efficient power allocation in green interference-alignment-based wireless networks," *IEEE Transactions on Vehicular Technology*, vol. 64, no. 9, pp. 4268–4281, 2015.

[35] X. Li, Y. Sun, F. R. Yu, and N. Zhao, "Antenna selection and power splitting for simultaneous wireless information and power transfer in interference alignment networks," in *2014 IEEE Global Communications Conference*, 2014, pp. 2667–2672.

[36] N. Zhao, F. R. Yu, and V. C. M. Leung, "Opportunistic communications in interference alignment networks with wireless power transfer," *IEEE Wireless Communications*, vol. 22, no. 1, pp. 88–95, 2015.

[37] ——, "Simultaneous wireless information and power transfer in interference alignment networks," in *2014 International Wireless Communications and Mobile Computing Conference (IWCMC)*, 2014, pp. 7–11.

[38] R. Gupta, A. K. Chaturvedi, and R. Budhiraja, "Improved rate-energy tradeoff for energy harvesting interference alignment networks," *IEEE Wireless Communications Letters*, vol. 6, no. 3, pp. 410–413, 2017.

[39] C. Yetis, T. Gou, S. Jafar, and A. Kayran, "On feasibility of interference alignment in MIMO interference networks," *IEEE Transactions on Signal Processing*, vol. 58, no. 9, pp. 4771–4782, 2010.

[40] Ó. González, C. Beltrán, and I. Santamaría, "A feasibility test for linear interference alignment in MIMO channels with constant coefficients," *IEEE Transactions on Information Theory*, vol. 60, no. 3, pp. 1840–1856, 2014.

[41] C. Wang, T. Gou, and S. a. Jafar, "Subspace alignment chains and the degrees of freedom of the three-user MIMO interference channel," *IEEE Transactions on Information Theory*, vol. 60, no. 5, pp. 2432–2479, 2014.

[42] G. Bresler, D. Cartwright, and D. Tse, "Settling the feasibility of interference alignment for the MIMO interference channel: the symmetric square case," *IEEE Transactions on Information Theory*, pp. 1–13, 2011.

[43] ——, "Feasibility of interference alignment for the MIMO interference channel," *IEEE Transactions on Information Theory*, vol. 60, no. 9, pp. 5573–5586, 2014.

[44] M. Razaviyayn, G. Lyubeznik, and Z.-Q. Luo, "On the degrees of freedom achievable through interference alignment in a MIMO interference channel," *IEEE Transactions on Signal Processing*, vol. 60, no. 2, pp. 812–821, 2012.

[45] N. Garg, A. K. Jagannatham, G. Sharma, and T. Ratnarajah, "Precoder feedback schemes for robust interference alignment with bounded csi uncertainty," *IEEE Transactions on Signal and Information Processing over Networks*, vol. 6, pp. 407–425, 2020.

[46] N. Zhao, F. Yu, and V. Leung, "Wireless energy harvesting in interference alignment networks," *IEEE Communications Magazine*, vol. 53, no. 6, pp. 72–78, 2015.

[47] Y. Li, L. Zhang, L. J. Cimini, and H. Zhang, "Statistical analysis of mimo beamforming with co-channel unequal-power mimo interferers under path-loss and rayleigh fading," *IEEE Transactions on Signal Processing*, vol. 59, no. 8, pp. 3738–3748, 2011.

[48] O. E. Ayach and R. W. Heath, "Interference alignment with analog channel state feedback," *IEEE Transactions on Wireless Communications*, vol. 11, no. 2, pp. 626–636, 2012.

[49] J. Kang, I. Kim, and D. I. Kim, "Wireless information and power transfer: Rate-energy tradeoff for nonlinear energy harvesting," *IEEE Transactions on Wireless Communications*, vol. 17, no. 3, pp. 1966–1981, 2018.

[50] X. Zhou, R. Zhang, and C. K. Ho, "Wireless information and power transfer: Architecture design and rate-energy tradeoff," *IEEE Transactions on Communications*, vol. 61, no. 11, pp. 4754–4767, 2013.